A comparison of numerical methods for the time domain modelling of pile driving noise in the near field

Daniel Ryan Wilkes[1]; Tim Gourlay[1]; Alexander Gavrilov[1]

[1] Centre for Marine Science and Technology (CMST), Curtin University, Perth, WA 6102, Australia

ABSTRACT

This paper presents a comparison of numerical methods for the modelling of pile driving noise in the near field of the pile. The numerical models considered consist of (1) an axisymmetric time domain finite difference method (FDM), developed by the Centre for Marine Science and Technology in the Matlab programming language, and (2) an axisymmetric time domain finite element method (FEM), which is available as part of the PAFEC–FE commercial software suite. The FDM employs thin-shell theory to model the cylindrical steel pile and the acoustic wave equation to model the water and fluid seabed, while the FEM employs the elastic and acoustic wave equations to model sound propagation in the pile and water/fluid seabed respectively. A one–way coupling of the pile displacements to the fluid pressures is utilised in the FDM to model the acoustic radiation from the pile excitation, while the FEM employs a fully coupled fluid-structure interaction at the solid–fluid interface. Numerical results for both models are presented in the form of pile radial displacement results and pressure results in the near field of the pile. Good agreement is observed between the FDM and FEM models, while the FDM is observed to be at least twice as fast as the FEM for the considered models.

Keywords: Pile driving, FEM, FDM I-INCE Classification of Subjects Number(s): 12.2.3, 75.3

1. INTRODUCTION

High-intensity impulsive underwater noise from marine pile driving may affect marine animals in the surrounding area. This may manifest as a physiological impact at shorter distances to the driven pile, or as a behavioural effect at larger distances (1). The impact distance depends on several parameters of the pile driving, such as the impact energy, and physical characteristics of the pile, and environmental parameters, such as the water depth, sediment composition and sound speed profile in the water. To prevent potential harm of pile driving to the marine fauna, the distances of physiological and behavioural impacts on different animals need to be determined.

The driving of a pile into the seabed constitutes a physically complex source of sound: the pile is struck by an impact hammer on the top end to drive the pile into the seabed, and so the impulsive hammer impact energy travels down the pile as a compressional wave, which also results in a shear deformation in the radial direction due to the Poisson effect. The pile deformation thus results in sound radiating into the water column and seabed via a coupled fluid–structure interaction (FSI), as well as directly into the seabed from the downward pile displacement. The pile itself is typically partially embedded in the seabed, partially submerged in the water column, and partially protrudes above the water line, and furthermore, will be partially filled with all 3 media (air, water and seabed material). To calculate the radiated underwater noise field, a numerical model, which can accurately represent the physical configuration of the pile driving scenario, is required (2).

Such pile driving configurations may be modelled with numerical techniques, such as the finite element method (FEM) and finite difference method (FDM), which both involve a numerical discretisation (of the physical domain in the former, and of the governing differential equations in the later (3)) and so allow for the geometry and material properties of the pile, water column and seabed to be explicitly included in the model. However the resolution of the discretisation is dictated by the highest frequency of interest (typically a few kHz for pile driving) which practically restricts these models to the near field (10's of m). Long range propagation of underwater pile driving noise to 10's of km or more may be achieved by inputting the calculated near field into an appropriate long range propagation model, as has been done for example by Reinhall and Dahl (4) (using a near field FEM coupled to a long range parabolic equation model) and Lippert et al. (5) (using a near

[1] D.Wilkes@curtin.edu.au
[2] T.Gourlay@cmst.curtin.edu.au
[3] A.Gavrilov@cmst.curtin.edu.au

field FEM coupled to a long range wavenumber integration model).

This paper presents a comparison of numerical results for axisymmetric time–domain FEM and FDM models in the near field, in the form of near field pressures and on–pile radial displacement results. The pile driving scenario used is essentially the same as that adopted in the recent COMPILE workshop on predicting offshore pile driving noise (6). The principal focus of this study is to determine the relative effect of the simplifying assumptions of the FDM model on the resulting near field pressure/displacement results, and so to ascertain the merit of coupling the near field FDM model (which is much faster to set up and solve than the FEM) to a long range propagation model for fast characterisation of the far field underwater pile driving noise. The FEM may then be used to model the near field for the more detailed pile driving scenarios of interest and/or more complex geometries. The paper is organised as follows: Section 2 presents the problem configuration for the pile driving modelling, Sections 3 and 4 present the background theory and solution methods for the FEM and FDM axisymmetric time–domain models respectively, Section 5 compares the numerical results for the two models, and finally Section 6 presents the conclusions.

2. PROBLEM CONFIGURATION

The modelled pile is a steel cylindrical tube 25 m in length, has an outer radius of 1 m and a wall thickness h of 0.05 m. The water column is modelled with a depth of 10 m and the pile is embedded 15 m into the seabed (i.e. making the top rim of the pile level with the sea surface). It should be noted that the seabed is treated as an equivalent fluid and so does not support shear waves or interface waves between the water and seabed. A schematic of the problem set up is shown in Fig. 1 in the axisymmetric (z,r) axial/radial coordinate system while the pertinent material properties of the involved media are presented in Table 1. This problem configuration is essentially the same as that specified for the COMPILE benchmark model (6). However the present time domain FEM/FDM models do not allow for the pile–sediment friction to be approximated by the frequency dependent absorption coefficients suggested in the COMPILE problem configuration and so this effect has not been included in the present models. Additionally the present FEM/FDM models restrain the radial degrees of freedom at the top of the pile to model the friction between the top of the pile and the impact hammer, while the COMPILE problem configuration does not specify such a condition.

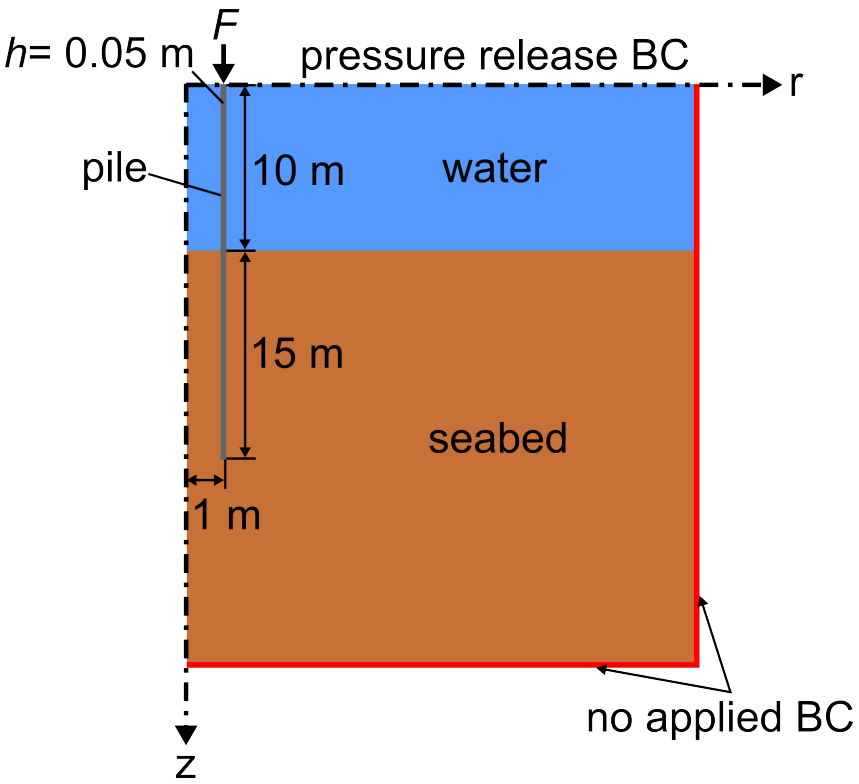

Figure 1 – Schematic of the pile driving model. The axis of symmetry for the axisymmetric coordinate system is defined at the pile centre ($r = 0$ m), a pressure release boundary condition (BC) is specified at the sea surface ($z = 0$ m) while no boundary condition is applied at the maximum axial and radial boundaries of the model. The maximum boundary dimensions are thus chosen to ensure that the leading wave front will not reach these boundaries over the time length of the simulation.

Table 1 – Material properties used for the pile driving model.

Parameter	Notation	Value	Unit
Density of steel pile	ρ_p	7850	$\mathrm{kg/m^3}$
Young's modulus of steel pile	E_p	210	GPa
Poisson's ratio of steel pile	ν_p	0.3	-
Density of water	ρ_w	1025	$\mathrm{kg/m^3}$
Sound speed in water	c_w	1500	$\mathrm{m/s}$
Density of fluid seabed	ρ_s	2000	$\mathrm{kg/m^3}$
Sound speed in fluid seabed	c_s	1800	$\mathrm{m/s}$

The hammer impact is modelled as a downward axial force F applied at the top of the pile. This forcing function is characterised by a sharp linear increase in the applied force followed by an exponential decay. The forcing function is defined as

$$F = \begin{cases} F_p \frac{t}{t_r} & \text{for } t \leq t_r \\ F_p e^{-\frac{t-t_r}{t_d}} & \text{for } t > t_r \end{cases} \tag{1}$$

where $F_p = 20$ MN, $t_r = 0.2$ ms and $t_d = 1.6$ ms. Thus a peak downward force of 20 MN is applied at 0.2 ms.

3. FEM

The axisymmetric time domain FEM model of the pile driving scenario has been implemented using the PAFEC–FE software suite, developed by PACSYS (7). At the boundary interface between the elastic steel pile and fluid media the boundary conditions require (a) continuity of the structural displacements/fluid particle velocities normal to the boundary surface and (b) the surface normal stresses and fluid pressures must be equal and opposite to one another (8). This yields a coupled FSI between the vectors of nodal structural displacements $\mathbf{u}$ and nodal pressures $\mathbf{p}$, which may be written as a discretised matrix equation

$$\begin{bmatrix} \mathbf{K}_s & \mathbf{C}^T \\ \mathbf{0} & \mathbf{K}_f \end{bmatrix} \begin{bmatrix} \mathbf{u} \\ \mathbf{p} \end{bmatrix} + \begin{bmatrix} \mathbf{D}_s & \mathbf{0} \\ \mathbf{0} & \mathbf{D}_f \end{bmatrix} \begin{bmatrix} \dot{\mathbf{u}} \\ \dot{\mathbf{p}} \end{bmatrix} + \begin{bmatrix} \mathbf{M}_s & \mathbf{0} \\ -\mathbf{C} & \mathbf{M}_f \end{bmatrix} \begin{bmatrix} \ddot{\mathbf{u}} \\ \ddot{\mathbf{p}} \end{bmatrix} = \begin{bmatrix} \mathbf{F}_s \\ \mathbf{0} \end{bmatrix} \tag{2}$$

where $\mathbf{K}$, $\mathbf{D}$ and $\mathbf{M}$ are the global stiffness, damping and mass matrices respectively for the steel pile (denoted by subscript s) and the combined water/fluid seabed (denoted by subscript f), ($\dot{\mathbf{u}}$,$\ddot{\mathbf{u}}$) and ($\dot{\mathbf{p}}$,$\ddot{\mathbf{p}}$) are the first and second time derivatives of the nodal displacement and pressure unknowns respectively, $\mathbf{C}$ is a coupling matrix which relates the displacement unknowns which are in contact with the fluid media to the coincident pressure unknowns and $\mathbf{F}_s$ is the vector of nodal forces applied to the pile (i.e. related to the hammer impact forcing function F for the nodes defining the top of the pile and defined as zero elsewhere) (9).

The solution of Eq. (2) in the frequency domain is straightforward: assuming a time dependence of the form $e^{-i\omega t}$ then the first and second time derivatives of the displacement/pressure unknowns are related by simple $-i\omega$ factors and so Eq. (2) constitutes an exactly solvable matrix equation for the ($\mathbf{u}$,$\mathbf{p}$) nodal unknowns. Conversely, Eq. (2) may be treated as an initial–value problem which can be solved in the time domain by marching the solution forward by a (usually fixed) time step Δt and solving Eq. (2) for the nodal displacement/pressure unknowns at each new time step using information from the prior time steps (3). The time domain recurrence algorithms are typically classified as either:

1. implicit schemes, where the discretised unknowns for the problem require a numerical solution of the FEM coupled matrix equation at each new time step which satisfy some constraints at both the new and the previously solved time steps, or
2. explicit schemes, where the unknowns at the new time step are explicitly calculated via simple matrix–vector products of the FEM coefficient matrices with the nodal solutions from the previous time steps.

Typically the implicit schemes are slower due to the numerical solution required at each time step, while the explicit schemes require a comparatively smaller time step for numerical stability (9). In this work PAFEC–FE's implicit solver, based on the Newmark–Beta method (10), is employed for the FEM model. For the coupled FEM system in Eq. (2) the Newmark–Beta recurrence relation for calculating the displacements/pressures at

the $n+1$th time step is

$$\left[\mathbf{M}+\gamma\Delta t\mathbf{D}+\beta\Delta t^2\mathbf{K}\right]\begin{bmatrix}\mathbf{u}_{n+1}\\ \mathbf{p}_{n+1}\end{bmatrix} = \left[2\mathbf{M}-(1-2\gamma)\Delta t\mathbf{D}-(1/2-2\beta+\gamma)\Delta t^2\mathbf{K}\right]\begin{bmatrix}\mathbf{u}_{n}\\ \mathbf{p}_{n}\end{bmatrix} - \left[\mathbf{M}-(1-\gamma)\Delta t\mathbf{D}+(1/2+\beta-\gamma)\Delta t^2\mathbf{K}\right]\begin{bmatrix}\mathbf{u}_{n-1}\\ \mathbf{p}_{n-1}\end{bmatrix} - \Delta t^2\left[\beta\mathbf{F}_{n+1}+(1/2-2\beta+\gamma)\mathbf{F}_n+(1/2+\beta-\gamma)\mathbf{F}_{n-1}\right] \quad (3)$$

where the non–subscripted **K**, **D** and **M** matrices and corresponding **F** vector denote the combined solid/fluid FEM coefficient matrices and force vector appearing in Eq. (2), and Eq. (3) is suitably modified for the initial time steps to begin the recursion. The β and γ parameters, as well as the time step Δt, should be carefully chosen to ensure a stable solution. In particular a choice of $\beta = 1/4$ and $\gamma = 1/2$ is known to provide an unconditionally stable solution (3). The typical time step criterion for *explicit* time marching schemes is

$$\frac{c\Delta t}{L} \leq 1 \quad (4)$$

where c denotes the compressional wave speed in the fluid or elastic solid and L is the internode distance for the finite elements. Eq. (4) can be recognised as the one dimensional case of the Courant condition for a Courant number of 1. An analogous criterion for the implicit time marching schemes seems to be less well defined, although it is generally agreed that the time steps for implicit schemes can be made somewhat larger than that specified by Eq. (4) without loss of accuracy. Upper limits to the time stepping criterion which are proportional to the maximum frequency component in the forcing function (f_m) are suggested for a number of implicit schemes, for example $\Delta t \leq \frac{1}{\pi f_m}$ in (3) and $\Delta t \leq \frac{1}{2f_m}$ in (11).

The pile driving configuration presented in Fig. 1 was implemented in PAFEC–FE using axisymmetric 6 node quadratic triangular displacement–based elements for the steel pile and similar pressure–based elements for the water/fluid seabed. A mesh discretisation of 2.5×10^{-2} m was used for the steel pile, while the fluid mesh was interpolated from an element size of 2.5×10^{-2} m at the pile interface to 0.4 m at the maximum radial distance of 85 m and maximum axial depth of 125 m, yielding a total mesh size of approximately 250 000 elements. The maximum dimensions of the FEM mesh were chosen to ensure that the leading pressure front radiated from the pile would not reach the outer mesh boundaries which do not have an applied boundary condition (red boundaries in Fig. 1) when running time domain simulations for up to 50 ms. A time step of 10 μs has been used for the FEM model, which satisfies the previously mentioned implicit time stepping criteria for a maximum frequency component in the forcing function limited to 2.5 kHz, as specified in the COMPILE benchmark model (6). The total solution time for the 50 ms FEM model was approximately 2.3 hours, with the dominant time cost from reading in the externally generated FEM mesh into PAFEC–FE. The implicit time stepping solution requires less than 20 minutes due to the recent incorporation of the PARDISO sparse symmetric solver (12) into the PAFEC–FE software suite. Previously the total solution time for much smaller FEM models was of the order of several days.

4. FDM

The axisymmetric time domain FDM model has been developed at CMST as an in–house Matlab code. The FDM code models the elastic steel pile using thin–shell theory (13), which assumes that the wall thickness h is small compared to the pile outer radius a. Greenspon (14) showed that thin-shell theory is suitable for cylindrical piles with $h/a < 0.1$, as is typically the case for offshore piles. The FDM is a linear theory, assuming that axial and radial displacements are small compared to the pile radius.

The governing equations follow (15), Eq. (7.80). We use coordinates z measured from the top of the pile and r measured from the pile centreline, and time t measured from the moment of impact. Axial displacement $u(z,t)$ and radial displacement $w(z,t)$ are then given by

$$\frac{\partial^2 u}{\partial t^2} = c_p^2\left(\frac{\partial^2 u}{\partial z^2}+\frac{\nu_p}{a}\frac{\partial w}{\partial z}\right) \quad (5)$$

$$\frac{\partial^2 w}{\partial t^2} = -c_p^2\left(\frac{\nu_p}{a}\frac{\partial u}{\partial z}+\frac{w}{a^2}\right)-\frac{p_a}{\rho_p h} \quad (6)$$

The elastic wave phase speed in a plate is (15)

$$c_p = \sqrt{\frac{E_p}{\rho_p \left(1-\nu_p^2\right)}} \tag{7}$$

In Eq. (6) we have omitted the bending term involving $\partial^4 w/\partial z^4$, as this was found to only negligibly affect the results for practical cases. Eq. (6) includes the effect of external loading through the fluid radiation pressure p_a.

For steel, the effect of material damping is very small, with damping being around 0.04–0.2% of the critical damping coefficient (16). We include material damping in equation (6) through a linear damping term, and this is found to decrease radial motion by around 1% by the time the leading wave has reached the bottom of the pile.

The equations of motion (5) and (6) for the pile without external loading are discretised using centred 2nd-order differencing to give

$$u_{j,n+1} = 2u_{j,n} - u_{j,n-1} + \left(\frac{c_p \Delta t}{\Delta z}\right)^2 \left(u_{j+1,n} - 2u_{j,n} + u_{j-1,n}\right) + \frac{\nu_p \left(c_p \Delta t\right)^2}{2a\Delta z}\left(w_{j+1,n} - w_{j-1,n}\right) \tag{8}$$

$$w_{j,n+1} = 2w_{j,n} - w_{j,n-1} - \frac{\left(c_p \Delta t\right)^2}{a} w_{j,n} - \frac{\nu_p \left(c_p \Delta t\right)^2}{2a\Delta z}\left(u_{j+1,n} - u_{j-1,n}\right) \tag{9}$$

Here $u_{j,n} = u\left(j\Delta z, n\Delta t\right)$, and similarly for w. A Von Neumann stability analysis reveals that Eqs. (8,9) are stable provided the Courant condition (Eq. (4) with $c = c_p$ and $L = \Delta z$) is satisfied.

With external loading, a Von Neumann stability analysis suggests that an explicit FDM similar to Eqs. (8,9) is universally unstable. Implicit schemes of this type have also been developed by CMST and found to be unstable in practice. Stability may be able to be achieved by including numerical damping, as is done in the FEM, and this is a topic for further research.

For the present, we use Eqs. (8,9) without external radiation loading, on the understanding that the density of steel is much higher than that of the water and seabed, so that the effect of radiation loading should be small. A correction is instead applied based on energy considerations, to be discussed later.

The applied pressure $F/\left(2\pi a h\right)$ from the impact hammer is incorporated at the top of the pile via the boundary condition

$$\frac{F}{\left(2\pi a h\right)} = -E_p \left.\frac{\partial u}{\partial z}\right|_{z=0} \tag{10}$$

The acoustic wave equation for the fluid (water or seabed) pressure p can also be solved using a finite difference method (3). In cylindrical coordinates, assuming axial symmetry, the acoustic wave equation is

$$\frac{\partial^2 p}{\partial t^2} = c^2 \left(\frac{\partial^2 p}{\partial z^2} + \frac{\partial^2 p}{\partial r^2} + \frac{1}{r}\frac{\partial p}{\partial r}\right) \tag{11}$$

Here c is the sound speed in the fluid (water or seabed). Applying centred differencing to Eq. (11) gives

$$\begin{aligned} p_{j,k,n+1} = {} & 2p_{j,k,n} - p_{j,k,n-1} + \left(\frac{c\Delta t}{\Delta r}\right)^2 \left(p_{j,k+1,n} - 2p_{j,k,n} + p_{j,k-1,n}\right) + \frac{\left(c\Delta t\right)^2}{2r\Delta r}\left(p_{j,k+1,n} - p_{j,k-1,n}\right) \\ & + \left(\frac{c\Delta t}{\Delta z}\right)^2 \left(p_{j-1,k,n} - 2p_{j,k,n} + p_{j-1,k,n}\right) \end{aligned} \tag{12}$$

Here $p_{j,k,n} = p\left(j\Delta z, a + k\Delta r, n\Delta t\right)$. A Von Neumann stability analysis shows that the stability of Eq. (12) is the same as that of the 2D wave equation in Cartesian coordinates, (17) p201. The method is stable provided

$$\left(\frac{c\Delta t}{\Delta r}\right)^2 + \left(\frac{c\Delta t}{\Delta z}\right)^2 \leq 1 \tag{13}$$

Two boundary conditions are applied at the water/seabed interface: the dynamic condition, which requires continuity of pressure; and the linearised kinematic condition (18) Eq. (2.72), which requires continuity of $\frac{1}{\rho}\frac{\partial p}{\partial z}$.

On the pile boundary, we apply the wall boundary condition (15) Eq. (6.35), i.e.

$$\left.\frac{\partial p}{\partial r}\right|_{r=a} = -\rho \frac{\partial^2 w}{\partial t^2} \tag{14}$$

where ρ is the density of either the water or fluid.

Without including radiation loading on the pile, the pile motion may be solved independently of the water and seabed, and the resulting pile motions are then used to drive the acoustic pressure through the wall boundary condition (14).

A useful check on any modelling method is to monitor the energy contained in the pile, water and seabed as a function of time. The energy in the hammer is also important, but this will not be discussed here. In the pile, kinetic energy density $\bar{E}_{\text{pile-kinetic}}$ is calculated, (19) Eq. 2.43, by

$$\bar{E}_{\text{pile-kinetic}} = \frac{\rho_p}{2}\left[\left(\frac{\partial u}{\partial t}\right)^2 + \left(\frac{\partial w}{\partial t}\right)^2\right] \tag{15}$$

Strain energy density $\bar{E}_{\text{pile-strain}}$ is calculated, (13) p192, by

$$\bar{E}_{\text{pile-strain}} = \frac{E_p h^2}{24\left(1-\nu_p^2\right)}\left[\left(\frac{\partial^2 w}{\partial z^2}\right)^2 + \frac{3h^2}{4}\left(\frac{\partial u}{\partial z} - \frac{w}{a}\right)^2 + \frac{6h^2\left(1-\nu_p\right)}{4}\frac{w}{a}\frac{\partial u}{\partial z}\right] \tag{16}$$

The total energy in the pile E_{pile} is therefore

$$E_{pile} = 2\pi a h \int \left(\bar{E}_{pile-kinetic} + \bar{E}_{pile-strain}\right) dz \tag{17}$$

In the water or seabed, the rate of transfer of energy to the fluid is (18)

$$\frac{dE_{\text{fluid}}}{dt} = 2\pi a \int p|_{r=a}\frac{\partial w}{\partial t} dz \tag{18}$$

The one–way coupling method described above violates conservation of energy, as no energy is lost from the pile while energy is transferred to the surrounding fluid. We can correct for this energy loss using a conservation of energy approach. Radial displacements are multiplied by a time-dependent factor which is slightly less than unity. The linearity of the governing equations requires that axial displacements and acoustic pressure are also multiplied by the same factor. The factor is calculated so that the pile/fluid system contains the same energy at each time step as the pile in vacuo.

The pile driving configuration presented in Fig. 1 was implemented in the MATLAB FDM code using an axial grid spacing of $\Delta z = 0.25$ m up to a maximum depth of 275 m and a radial grid spacing of $\Delta r = 6.92 \times 10^{-2}$ m up to a maximum radial distance of 77 m, giving a total grid size of $[1101 \times 1101]$ points. As with the FEM, the maximum radial dimension of the FDM grid was chosen to ensure that the leading pressure front radiated from the pile will not reach the outer boundaries of the grid when running time domain simulations for up to 50 ms. A time step of 23 μs has been used for the FDM model, which can be seen to satisfy Eq. (13) for the compressional wave speed of either the water or fluid seabed. The total solution time for the 50 ms FDM model was approximately 1.3 hours.

5. RESULTS

This section presents numerical results for the COMPILE pile driving problem configuration described in Section 2 from both the PAFEC–FE FEM model, and CMST's FDM model. The numerical results are presented in the form of 'snapshots' of the radial displacements and pressures on the outer pile surface ($r = 1$ m), as well as similar results for the near field pressures at a radial distance of $r = 11$ m.

In addition to the 'coupled' FEM results, which incorporate the coupled FSI between fluid and structure, and the FDM results, which incorporate a one–way coupling and energy balancing method, results for a one–way (or 'uncoupled') FEM model are also shown at each time step. The uncoupled FEM results were calculated using PAFEC–FE by first solving for the in–vacuo pile displacements which are then used as inputs for the fluid FEM model to calculate the radiated sound pressure from the pile (i.e. ignoring the FSI). The purpose of presenting the uncoupled FEM models is to investigate the relative effect of the simplifying assumptions of the FDM model — particularly the one–way coupling and energy balancing technique and thin–shell theory employed in the FDM model. The uncoupled FEM employs a similar one–way coupling technique as the FDM but does not make the thin–shell assumptions, thus allowing for a separate analysis of the effect of the two assumptions on the results.

The radial displacements on the outer pile surface calculated by the coupled/uncoupled FEM and FDM models are presented in Fig. 2, for a series of time steps ranging from 2 ms to 10 ms. Each time snapshot is

shown over the length of the pile (y–axis) from 0 m at the sea surface to 25 m at the bottom of the pile, while the radial displacements are shown on the x–axis in metres. These time steps show the radial shear deformation of the pile due to the compressional wave excited by the hammer impact travelling down to the bottom of the pile, reflecting, and returning back to the top of the pile. In each subplot the black arrow indicates the approximate position of the main compressional wave, as evidenced by the large positive or negative displacement peaks calculated by all models. The uncoupled FEM and FDM models can be seen to be in good agreement at all time steps, while both uncoupled models differ from the coupled FEM results. Some notable differences are also observed between the uncoupled models in the radial deformation from the main compressional wave at the later time steps, with the FDM model exhibiting progressively smaller peak displacements over time. This is due to the energy balancing method employed by the FDM progressively reducing the radial displacements over time as energy is radiated into the water column/seabed. Both sets of FEM results show small oscillations on top of the main deformation that propagate at a slow velocity down the length of the pile (these can be seen developing at $t = 4$ ms at 5 m depth) and so are likely higher order flexural modes which are being excited in the FEM models. Clearly the radial displacements from these waves are comparatively small compared to the radial deformation from the main compressional wave. The added fluid loading in the coupled FEM models dampens the radial vibrations, with the main compressional wave broadening, and its amplitude decaying faster than that of the uncoupled models. The initial radial displacements of the coupled FEM model are also smaller than that of the uncoupled models. It is concluded that the observed differences between the uncoupled FEM/FDM and coupled FEM models is likely due to the FSI, while the use of the simplified thin–shell theory in the FDM model yields very similar results to the uncoupled FEM (which employs the axisymmetric form of the elastic wave equation).

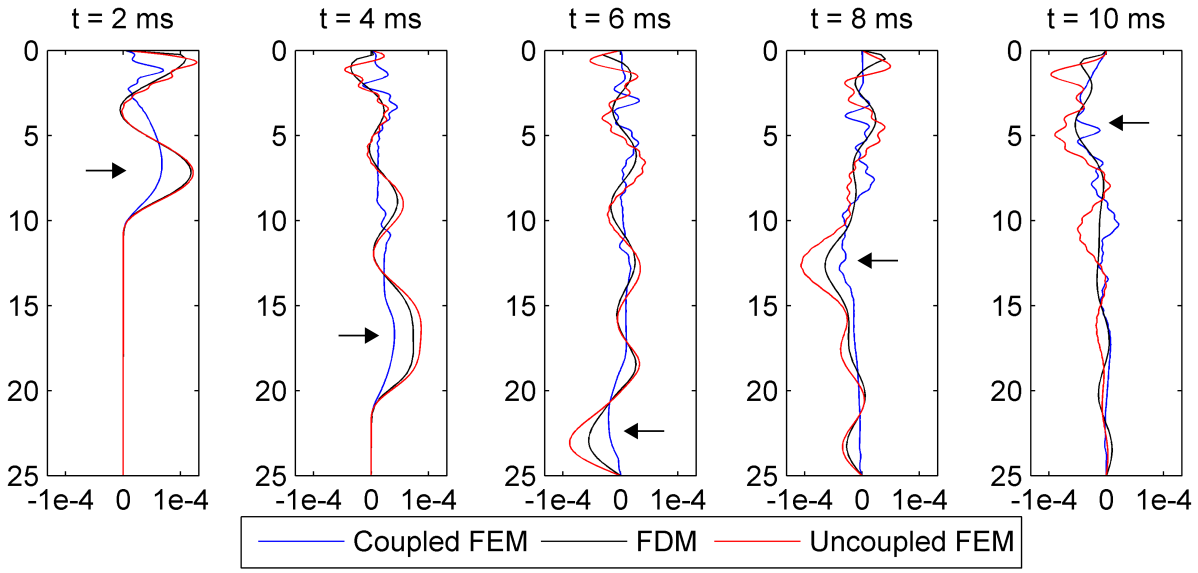

Figure 2 – Radial displacement on the outer pile surface from the FEM and FDM models for a series of time steps ranging from 2 ms to 10 ms. In each plot the vertical y–axis indicates depth (in m) from the sea surface and the horizontal x–axis indicates the radial displacement (in m). The black arrows in each plot mark the approximate position of the main compressional wave excited by the hammer impact.

The pressures on the outer pile surface calculated by the coupled/uncoupled FEM and FDM models are presented in Fig. 3 using a similar format to Fig. 2 (i.e. with the length of the pile from 0 to 25 m depth on the y–axis and the pressure in Pascals on the x–axis), again presented for a series of time steps ranging from 2 ms to 10 ms. The black arrows in the 2 and 4 ms plots mark the approximate position of the peak fluid pressures corresponding to the main compressional wave travelling down the length of the pile. The excited peak pressure is travelling faster than the fluid sound speed and so results in a downward angled wavefront radiating into the water column/fluid seabed, corresponding to the first downward travelling Mach cone identified by Reinhall and Dahl (4). The upward travelling wave/Mach cone can be identified in the 6 ms plot, after which it is more difficult to identity it within the secondary downward travelling waves. The differences between the coupled FEM and FDM results is again likely due to the coupled FSI effect. Good agreement is again observed between the uncoupled FEM and FDM models. The coupled FEM model can be seen to yield smaller peak pressures in the main compressional wave which then decay in amplitude faster than the uncoupled FEM/FDM models (as was the case with the coupled FEM radial displacements).

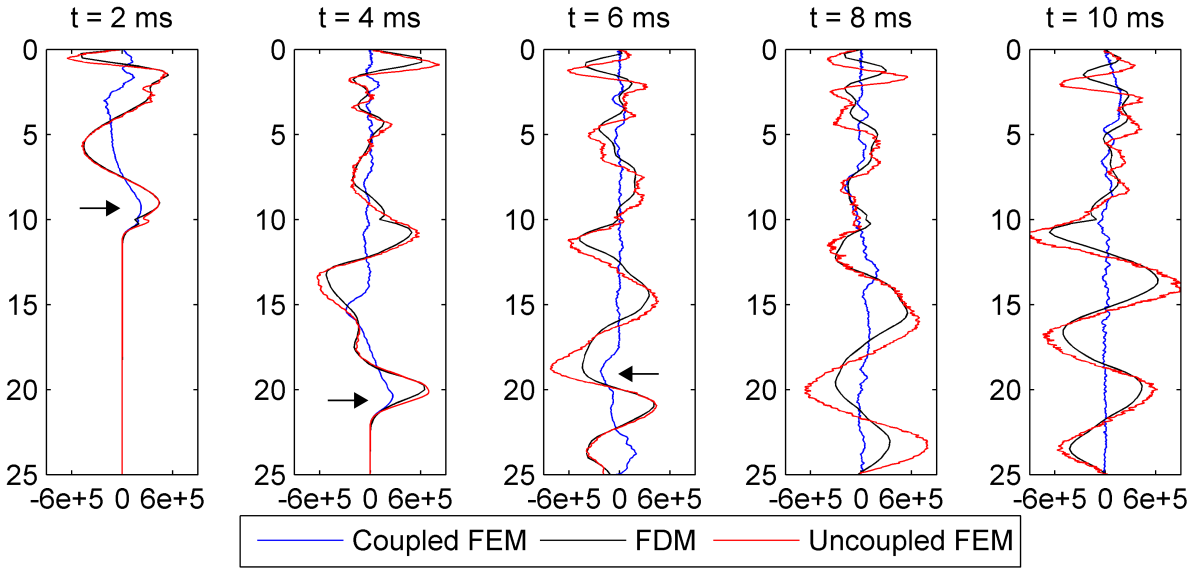

Figure 3 – Pressure on the outer pile surface from the FEM and FDM models for a series of time steps ranging from 2 ms to 10 ms. In each plot the vertical y–axis indicates depth (in m) from the sea surface and the horizontal x–axis indicates the pressure (in Pa). The black arrows in the 2, 4 and 6 ms plots mark the approximate position of the peak pressures due to the main compressional wave from the hammer impact. These points correspond to the on–pile positions for the first downward and upward travelling Mach cones.

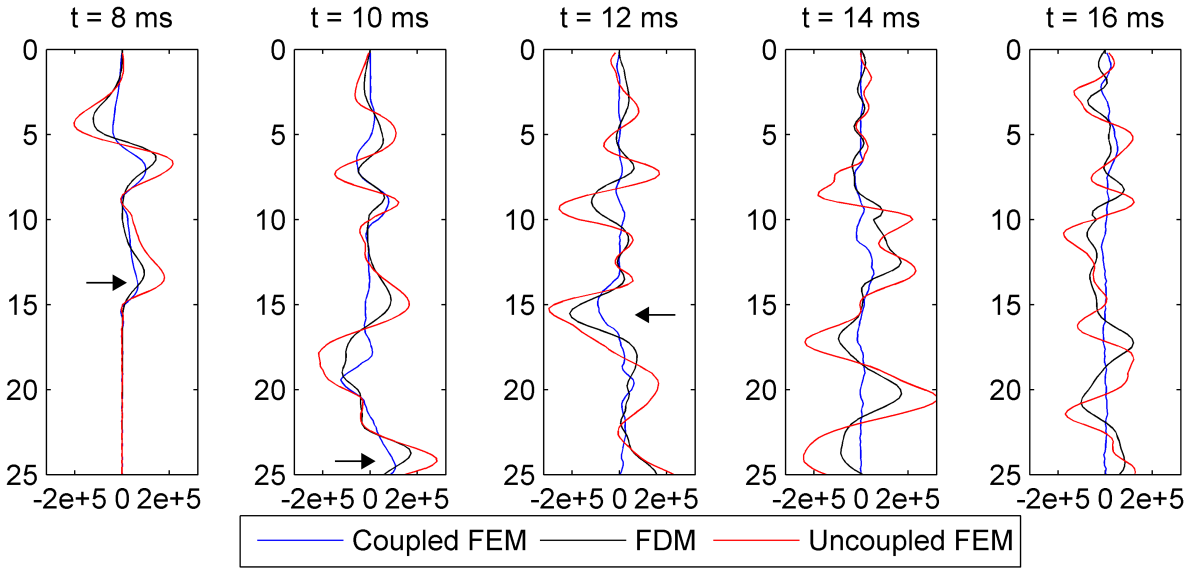

Figure 4 – Pressure at $r = 11$ m for the FEM and FDM models for a series of time steps ranging from 8 ms to 16 ms. In each plot the vertical y–axis indicates depth (in m) from the sea surface and the horizontal x–axis indicates the pressure (in Pa). The peak pressures of the first downward and upward travelling Mach cones can be seen in the 8/10 ms and 12 ms results respectively (marked with black arrows).

Fig. 4 shows the near field pressures over the depth range of the pile from the coupled FEM and FDM models at a radial distances of $r = 11$ m (i.e. 10m from the outer pile surface). The first Mach cone radiated from the pile takes approximately 6.5 ms to propagate to this distance and so the series of time steps is shown from 8 ms to 16 ms. The plot configuration is the same as in Fig 3 (y–axis: depth in metres and x–axis: pressure in Pascals). The peak pressure from the main wavefront of the first downward travelling Mach cone being radiated into the water column/fluid seabed can be identified in the 8 and 10 ms results (marked with black arrows) while the peak pressure of the first upward travelling Mach cone can be seen in the 12 ms results (similarly marked with a black arrow). The coupled FEM results again show lower peak pressures than the uncoupled FEM/FDM results and similarly decay in amplitude faster than those from the uncoupled models. Agreement between the uncoupled FEM and FDM results is again reasonable, with the uncoupled FEM generally predicting larger peak pressures than the FDM, while both models predict larger peak pressures and larger secondary oscillations propagating behind the main compressional wave as compared to the coupled FEM model.

Finally Fig. 5 show a snapshot of the pressure fields calculated by the coupled FEM and energy–balanced FDM models at a time step of 30 ms. The plots of these results have been generated using different software packages and so the colour tables cannot be exactly matched, but the pressure range used in both plots is identical. The downward/upward propagating Mach cones radiated from the pile can be seen in similar locations in both sets of results, while the FDM results again exhibit a much stronger interference pattern in the secondary waves propagating behind each Mach cone wavefront compared to the FEM results (as was observed in Fig. 4). The FDM results also exhibit generally larger amplitudes in the pressure field compared to the coupled FEM results, as was the case for the time snapshots presented in Figs. 3 and 4.

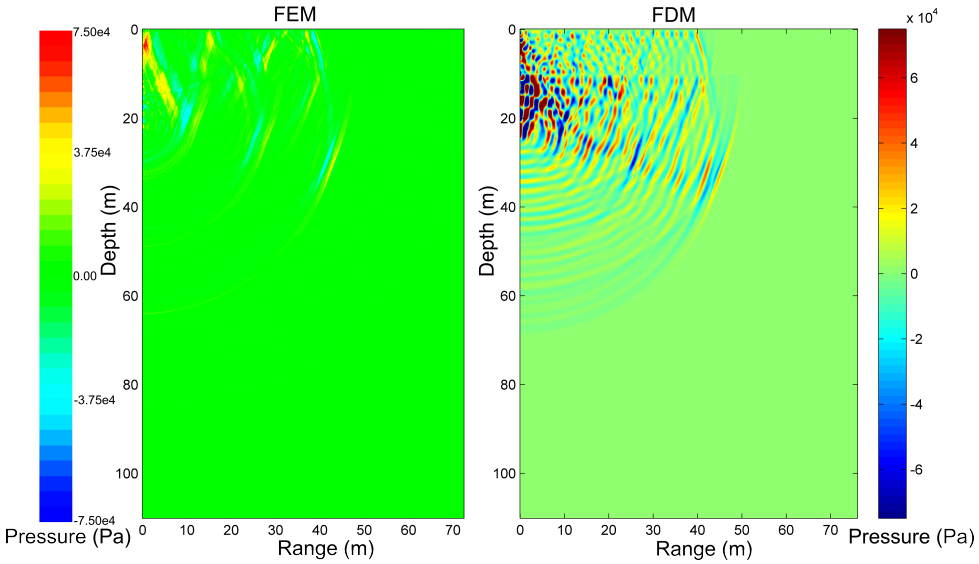

Figure 5 – Pressure fields calculated by the coupled FEM and FDM models at a time step of 30 ms. The downward and upward propagating Mach cones are clearly visible in both sets of results.

6. CONCLUSIONS

This paper has presented a comparison of numerical results of underwater pile driving noise from both an axisymmetric time domain FDM model and an axisymmetric time domain FEM model. The FDM model employs thin–shell theory to model the cylindrical steel pile and a one–way coupling and energy balancing method to model the acoustic radiation from the pile excitation, while the FEM employs the axisymmetric form of the elastic wave equation and a fully coupled FSI between the pile displacements and fluid pressures. Results from an uncoupled FEM model were also presented to allow for an independent evaluation of the simplifying assumptions used in the FDM model. A very good agreement between the FDM and uncoupled FEM displacements indicated that the use of the simplified thin–shell theory to model the pile in the FDM in lieu of the elastic wave equation is justified. The observed differences in the coupled FEM and FDM models were thus attributed to the coupled FSI effect. Pertinent features of the coupling effect were identified to be smaller initial radial displacements and fluid pressures (due to the added fluid loading on the pile), which then decayed in amplitude more quickly than the uncoupled FDM results. Future work will focus on modifying the pile model to more realistic scenarios, for example by extending the pile above the sea surface, including

an elastic seabed and including the pile–seabed friction effects into the model. Further development of the numerical models is also planned, such as investigating the stabilisation of the coupled FSI FDM model via the inclusion of damping, as well as coupling the models to a suitable long range propagation model to calculate the radiated noise from pile driving in the far field. Some work has already been conducted into the coupling of the near and far field models for the results presented by CMST at the recent COMPILE workshop.

7. ACKNOWLEDGEMENTS

The authors would like to thank Dr. Patrick Macey from PACSYS for his ongoing technical support and FEM knowledge in modelling the pile driving models in PAFEC–FE, and Dr. Alec Duncan (CMST) for his insightful discussions on the pile driving modelling, as well his useful feedback on the first draft of this paper.

REFERENCES

1. Erbe C. Underwater noise from pile driving in Moreton Bay, QLD. Acoust Aust. 2009;37(3):87–92.
2. Lippert T, Lippert S. Modelling of pile driving noise by means of wavenumber integration. Acoust Aust. 2012;40(3):178–182.
3. Jensen FB, Kuperman FA, Porter MB, Schmidt H. Computational Ocean Acoustics. AIP Series in Modern Acoustics and Signal Processing. New York: Springer-Verlag; 2000.
4. Reinhall PG, Dahl PH. Underwater Mach wave radiation from impact pile driving: Theory and observation. J Acoust Soc Am. 2011;130(3):1209–1216.
5. Lippert T, Heitmann K, Ruhnau M, Lippert S, von Estorff O. On the prediction of pile driving induced underwater sound pressure levels over long ranges. In: ICSV20: 20th International Congress on Sound and Vibration. Bangkok, Thailand; 2013. .
6. Lippert S, Ruhnau M. COMPILE: International benchmark study on the prediction of offshore pile driving noise; 2014. Available from: `http://bora.mub.tuhh.de/compile/`.
7. PACSYS: FEA / BEM Solutions; 2014. Available from: `http://www.vibroacoustics.co.uk/`.
8. Amini S, Harris PJ, Wilton DT. Coupled Boundary and Finite Element Methods for the Solution of the Dynamic Fluid-Structure Interaction Problem. Brebbia CA, Orszag SA, editors. no. 77 in Lecture Notes in Engineering. Berlin: Springer-Verlag; 1992.
9. Macey P. Finite element methods for transient acoustic analysis of audio problems. In: Proceedings of the Institute of Acoustics. vol. 25. Oxford, UK; 2003. .
10. Newmark NM. A method for computation of structural dynamics. Proc Am Soc Civ Eng. 1959;EM3:67–94.
11. Strommen EN. Structural Dynamics. vol. 2 of Springer Series in Solid and Structural Mechanics. Fremond M, Maceri F, editors. Springer; 2014.
12. PARDISO 5.0.0 Solver Project. http://www.pardiso-project.org/; 2014.
13. Love AEH. A Treartise on the Mathematical Theory of Elasticity. Cambridge University Press; 1893.
14. Greenspon JE. Vibrations of thick and thin cylindrical shalls surrounded by water. J Acoust Soc Am. 1961;33(10):1321–1328.
15. Junger MC, Feit D. Sound, Structuret and Their Interaction. Acoustical Society of America; 1993.
16. Stevenson JD. Structural damping values as a function of dynamic response stress and deformation levels. Nucl Eng Des. 1980;60:211–237.
17. Mitchell AR. Computational Methods in Partial Differential Equations. Wiley; 1969.
18. Tolstoy I, Clay CS. Ocean Acoustics: Theory and Experiment in Underwater Sound. Acoustical Society of America; 1987.
19. Kraus H. Thin Elastic Shells. John Wiley & Sons; 1967.